High Performance Magnesium Electrochemical Cycling with Hybrid Mg-Li Electrolytes

Melinda Krebsz,[†,*] Sam Johnston,[†] Cuong Ky Nguyen,[†] Yvonne Hora,[#] Binayak Roy,[†] Alexandr N. Simonov,[†,‡,*] and Douglas R. MacFarlane [†,‡]

[†] School of Chemistry, [#]Department of Chemical and Biochemical Engineering, and the [‡]ARC Centre of Excellence for Electromaterials Science, Monash University, Victoria 3800, Australia

*Corresponding Authors:

E-mails: melinda.krebsz@monash.edu (MK), alexandr.simonov@monash.edu (ANS)

Twitter: @KrebszMelinda (MK), @Simonov_A_N (ANS), @DRMacFarlane (DRM)

Abstract

Kinetics and coulombic efficiency of the electrochemical magnesium plating and stripping processes are to a significant extent defined by the composition of the electrolyte solution, optimisation of which presents a pathway for improved performance. Adopting this strategy, the current work presents a systematic investigation of the $Mg^{0/2+}$ process in different combinations of the Mg^{2+}–Li^{+}–borohydride–bis(trifluoromethanesulfonyl)imide ($TFSI^{-}$ or NTf_2^{-}) electrolytes in 1,2-dimethoxyethane (DME) solvent. Results indicate that the presence of BH_4^{-} is essential for high coulombic efficiency, which coordination to Mg^{2+} was confirmed by Raman and NMR spectroscopic analysis. However, the high rates observed also require the presence of Li^{+} and a supplementary anion like $TFSI^{-}$. The Li^{+} + BH_4^{-} + $TFSI^{-}$ combination of ionic species prevents passivation of the magnesium surface and thereby enables efficient $Mg^{0/2+}$ electrochemical cycling. The best $Mg^{0/2+}$ performance with the stabilised columbic efficiency of 88 ± 1% and one of the highest deposition/stripping rates at ambient temperature reported to date are demonstrated at an optimal $[Mg(BH_4)_2]$: [LiTFSI] mole ratio of 1 : 2.

Introduction

The natural abundance of magnesium[1] and the high theoretical volumetric energy density of Mg-metal batteries[1, 2] motivate investigations into this technology as an alternative to the traditional energy storage devices.[2-10] The key roadblock to the translation of Mg-batteries towards practical applications is the partial irreversibility of the electrochemical magnesium deposition/stripping cycle, *i.e.* notably the lower than 100% coulombic efficiency of the $Mg^{0/2+}$ cycling process that is often observed (Table 1). To a significant extent, this inefficiency is defined by the chemical properties of the solvent and electrolyte salt, which optimisation presents a clear pathway towards high-performance magnesium batteries. For example, as early as in 2000, organohaloaluminate-based Mg-electrolytes were introduced by Aurbach *et al.* to achieve a close to 100% columbic efficiency of the electrochemical magnesium cycling.[3, 11] On the downside, such electrolytes are highly corrosive and sustain only moderate magnesium electrodeposition/stripping rates. The latter is often compared in terms of the oxidative peak current density in cyclic voltammetry at a scan rate of 0.020 V s^{-1} recorded down to a specific negative reverse potential (E_{nr} / V *vs.* $Mg^{0/2+}$) (which is referred to as $j_{E_{nr}}$ henceforth). In the study by Aurbach *et al.*[3], $j_{-1.0}$ was only *ca.* 1 mA cm^{-2}.

A well-recognised reason for the low chemical reversibility of the $Mg^{0/2+}$ cycling is strong susceptibility of the process to even negligible amounts of water, which readily reacts with Mg^0 to produce an insulating and insoluble magnesium (hydr)oxide.[12] This is reflected in the very low rates and coulombic efficiency of the electrochemical magnesium deposition/stripping achieved with conventional electrolytes like magnesium(II) bis(trifluoromethanesulfonyl)imide ($TFSI^-$; also known as NTf_2^-)[13] in the presence of measurable amounts of H_2O (Table 1). The recognition of the pernicious effects of water motivated researchers to implement additional measures for its elimination. One possible strategy is to use $Mg(BH_4)_2$ as a component of the electrolyte, which is inherently an efficient water scavenger that can be expected to naturally purify the solution from any residual H_2O (resulting in an inevitable but small loss of the anion to insoluble borates) and subsequently enable improved electrochemical performance. Indeed, continuous $Mg^{0/2+}$ cycling was demonstrated on Pt electrodes using $Mg(BH_4)_2$ solutions in polyether solvents, but at low deposition rates (Table 1).[2, 8, 14] Moreover, even these rates and reasonably high coulombic efficiencies required operating the electrochemical cell at elevated temperature, majorly because the conductivity of the $Mg(BH_4)_2$ solutions in the tetraglyme solvent employed in this study is low.[2] The latter aspect can be improved by changing the solvent to an ionic liquid[14] or

a mixture of an ionic liquid with a molecular solvent,[8] though this approach still does not enable very high rates of Mg^0 deposition (Table 1).

Further development of this strategy emerged through the use of other than borohydride magnesium salts as the major electrolyte salt, for example $Mg(TFSI)_2$, while still keeping the H_2O scavenging component present. The latter can be the same $Mg(BH_4)_2$ salt[15] or other compounds like magnesium triphenolateborohydride[16] and heptamethyldisilazane.[17] Although the use of such mixed electrolytes does provide significant improvements, as compared to pure $Mg(TFSI)_2$ solutions, the coulombic efficiency of the process still remains below 100% (Table 1).

One of the most promising approaches to improve the magnesium cycling is based on the addition of lithium salts to the magnesium electrolyte solutions. In particular, this was previously investigated for $Mg(BH_4)_2$ in combination with $LiBH_4$.[2, 7-9, 18-20] Much higher $Mg^{0/2+}$ electrodeposition/stripping rates were achieved with such mixed electrolytes as compared to pure $Mg(BH_4)_2$ systems (Table 1). It is likely that this improvement is supported by enhanced ionic conductivity, though there might be other, yet to be unambiguously established, effects of the presence of Li^+ salts on the solid-electrolyte-interface (SEI) that facilitates the process. The chemical nature of solvent is also important, as demonstrated by Mohtadi *et al.*[18] in their study on the $LiBH_4$ + $Mg(BH_4)_2$ mixed electrolyte system that enabled higher current density at lower overpotentials for $Mg^{0/2+}$ electroreduction in 1,2-dimethoxyethane (DME) as compared to tetrahydrofuran. Based on the Fourier transform infrared spectroscopy (FTIR) analysis and improvements in the coulombic efficiency at higher $LiBH_4$ concentrations, the authors suggested that the electrochemical performance of the system could be additionally improved by weakening the ion pairing between Mg^{2+} and BH_4^- induced by the introduction of Li^+.[18] They have also confirmed that $Mg^{0/2+}$ was the dominant faradaic process by X-ray diffraction (XRD) analysis after galvanostatic electrodeposition experiments at -1 V *vs.* $Mg^{0/2+}$ and by demonstrating the scaling of the current density with the concentration of $Mg(BH_4)_2$.

Although the $Mg(BH_4)_2$ + $LiBH_4$ system enables reversible magnesium cycling with close to 100% coulombic efficiency, its application in batteries might be problematic due to the use of large amounts of borohydride, which is a highly reactive reductant and would react with many cathode materials. Replacing a significant part of the BH_4^- ions, therefore, seems to be a logical step in further developments to the system. The feasibility of this approach was demonstrated by Hebié *et al.*[16] for the 0.5 M $Mg(TFSI)_2$ + 0.5 M $LiBH_4$ and 0.5 M $Mg(TFSI)_2$ + 0.3 M $LiB(OPh)_3H$ mixed systems, both providing respectable magnesium reduction/stripping rates (Table 1). Unfortunately, the reported coulombic efficiency of the $Mg^{0/2+}$ process was

lower than 80% in both of these electrolyte solutions, which calls for deeper investigation into the factors affecting the performance of these promising mixed systems.

Table 1. Comparison of the properties of selected $Mg(BH_4)_2$ and $Mg(TFSI)_2$ electrolyte systems for $Mg^{0/2+}$ electrochemical cycling (data at room temperature unless otherwise noted).

Electrolyte[a]	**Solvent**[a]	σ [b] / mS cm^{-1}	**WE** [c]	E_{nr} [d] / V *vs.* $Mg^{0/2+}$	$j_{E_{nr}}$ [d] / mA cm^{-2}	**CE** [e] / %	**Ref**
0.5 M $Mg(TFSI)_2$	TGM	n.a.[f]	Pt	-0.8	0.4 (5)	38	13
0.5 M $Mg(BH_4)_2$	TG (90 °C)	0.038	Pt	-1.0	*ca*. 0.28[g](50)	n.a.	2
0.5 M $Mg(BH_4)_2$	$[MPEG_7Pyr][TFSI]$	n.a.	Pt	-1.0	2 (25)	90	14
0.5 M $Mg(BH_4)_2$	$[PP_{14}TFSI]$ + TG	1.3	Pt	-1.0	11 (50)	n.a.	8
0.5 M $Mg(TFSI)_2$ + 6 mM $Mg(BH_4)_2$	TG	n.a.	Pt	-0.6	2 (25)	75	15
0.5 M $Mg(TFSI)_2$ + 2 wt.% HpMS	TGM	*ca*. 2.5	Pt	-1.5	60 (20)	66	17
0.5 $Mg(TFSI)_2$ + 0.15 M $Mg[B(OPh)_3H]_2$	DGM	5.5	Pt	-1.0	20 (50)	64	16
0.18 M $Mg(BH_4)_2$ + 0.6 M $LiBH_4$	DME	*ca*. 2.2[g]	Pt	-1.0	26 (5)	94	18, 20
0.1 M $Mg(BH_4)_2$ + 1.5 M $LiBH_4$	DGM	3.3	Pt	-0.5	13 (20)	*ca*. 100	7
0.1 M $Mg(BH_4)_2$ + 1.5 M $LiBH_4$	DGM	n.a.	Pt	-0.8	2 (20)	*ca*. 100	19
0.5 M $Mg(BH_4)_2$ + 1.5 M $LiBH_4$	TG (90 °C)	9.7	Pt	-1.0	2 (50)	n.a.	2
0.5 M $Mg(TFSI)_2$ + 0.5 M $LiBH_4$	DGM	n.a.	Pt	-1.0	40 (100)	78	16
0.5 $Mg(TFSI)_2$ + 0.3 $LiB(OPh)_3H$	DGM	n.a.	Pt	-1.0	18 (100)	73	16
0.2 M $Mg(BH_4)_2$ + 0.4 M LiTFSI	DME	6.8	Pt	-0.5	27 (20)	89	**This work**[h]
			Pt	-0.8	48 ± 2 (20)	88 ± 1	
			Pt	-1.0	65 (20)	88	
			Cu	-0.8	30 ± 3 (20)	88 ± 2	
			Cu	-1.0	40 (20)	88	

[a] DME: glyme (1,2-dimethoxyethane), DGM: diglyme (1-methoxy-2-(2-methoxyethoxy)ethane), TGM: triglyme (1,2-bis(2-methoxyethoxy)ethane), TG: tetraglyme (2,5,8,11,14-pentaoxapentadecane), HpMS: heptamethyldisilazane, $[MPEG_7Pyr][TFSI]$: methoxypolyethylene glycol bis(trifluoromethylsulfonyl)imide, $PP_{14}TFSI$: 1-butyl-1-methylpiperidinium bis(trifluoromethyl sulfonyl)imide, $Mg[B(OPh)_3H]_2$: magnesium triphenolateborohydride. $LiB(OPh)_3H$: lithium triphenolateborohydride. [b] Conductivity. [c] Working electrode. [d] Negative reversal potential in cyclic voltammetry (E_{nr}) and Mg^0 oxidation peak current density measured in the positive voltammetric sweep after cycling down to E_{nr} ($j_{E_{nr}}$); scan rate in mV s^{-1} is provided in parentheses. [e] Coulombic efficiency of the $Mg^{0/2+}$ cycling calculated from the voltammetric data. [f] Not available. [g] Estimated from the plotted data. [h] Data corresponding to 10th voltammetric cycles (see Table S1-S3 for extended data).

Aiming to further contribute to the understanding of the parameters affecting the electrochemical $Mg^{0/2+}$ cycling in the presence of Li^+, the present work systematically investigates the hybrid magnesium–lithium–borohydride–$TFSI^-$ electrolytes, with the specific focus on the effects of the chemical nature and relative concentrations of the anion and cation. Through the optimisation of these parameters, we eventually achieve one of the highest rates and coulombic efficiencies yet reported for the $Mg^{0/2+}$ process.

Experimental

Materials. Lithium bis(trifluoromethanesulfonlyl)imide (LiTFSI, Fluorad™, HQ-115) was obtained from 3M. Magnesium borohydride (95%), lithium borohydride (≥90%), 1,2-dimethoxyethane (glyme; DME) (anhydrous, 99.5%) and magnesium ribbon (≥99.5%) were purchased from Sigma-Aldrich. Magnesium(II) bis(trifluoromethanesulfonyl)imide ($Mg(TFSI)_2$; 99.5%) was purchased from Solvionic. Lithium 1,1,1,3,3,3-(tetrakis)hexafluoroisopropoxy borate (LiBHfip) was prepared by exactly following the published procedure using the same reagents.[21] Trihexyltetradecylphosphonium bis((trifluoromethyl)sulfonyl)imide ($[P_{6,6,6,14}][TFSI]$) was synthetised by a methathesis reaction reported previously[22] using LiTFSI as a $TFSI^-$ source. Zeolite 1.5-2.5 mm beads with an average pore size of 4 Å were purchased from High Vacuum Technologies PL. Copper wire (99.8%) with a diameter of 1.25 mm was purchased from Fisher Scientific. All reagents and solutions were stored and handled inside a glove-box (KOREA KIYON glovebox system) under high purity argon (99.997%, O_2 < 1 ppm, H_2O < 1 ppm; sourced from BOC).

Prior to use, DME was dried over cleaned (washed several times with water and acetone) and freshly activated (48 h at 300 °C in air) zeolite (3 Å; Sigma-Aldrich) inside the Ar-filled glove-box. After initial drying, the zeolite was replaced with a fresh portion for storage of the solvent. The concentration of water in dried DME was determined by the Karl-Fisher method, and did not exceed *ca.* 0.3 mM (5 ppm). $Mg(TFSI)_2$ and LiTFSI were dried under vacuum at 80 °C for 48 h prior to the introduction to the glove-box, while $Mg(BH_4)_2$ and $LiBH_4$ were used as purchased.

Electrochemical experiments. Biologic VMP electrochemical workstation was used for the electrochemical measurements, all of which were undertaken inside an Ar-filled glove-box at ambient temperature (23 ± 2 °C) with no stirring. For each experiment, a new one-compartment 20 mL scintillation vial was employed as an electrochemical cell. Large surface area

magnesium ribbon (*ca.* 70 mm × 3.4 mm × 0.2 mm) was scraped with a scalpel to obtain clean and fresh electrode surface prior to each experiment and was used as a counter and reference electrode, *i.e.* experiments were undertaken in a two-electrode mode. All potentials reported herein are raw values measured against the magnesium ribbon counter/reference electrode, which was assumed to correspond to the $Mg^{0/2+}$ redox process under conditions employed.

As a working electrode, either a custom-made copper metal disk (diameter Ø 1.6 mm) embedded in a polyether ether ketone (PEEK) sheath or a platinum disk (Ø 1 mm) embedded in a PEEK sheath (BAS) was used. Before experiments, working electrodes were polished using a polishing emery paper and an aqueous slurry of 0.3 μm Al_2O_3 powder; the surface of the working electrode was further cleaned by rinsing with water and acetone, wiped over the clean polishing emery paper, washed again with acetone and finally dried in vacuum oven at 60 °C. In some experiments, a small piece of a Mg ribbon (pretreated inside the glove-box as described above) with an active surface area of 0.7 cm^2 was used as a working electrode. All currents reported herein are normalised to the geometric surface area of the working electrodes.

For physical characterisation of the reduction product, a non-isolated copper wire (Ø 1.25 mm; *ca.* 0.114 cm^2 geometric surface area) was used as a working electrode. In this case, the pretreatment of the working electrode included an oxidative electropolishing in concentrated orthophosphoric acid solution (at 4 A current for 2 min) using the setup and following the procedure described in the literature.[23] After pretreatment, the electrode was rinsed with water, washed with ethanol and dried before it was introduced into the glove-box.

Physical characterisation

Raman spectra were recorded using a Renishaw Raman spectrometer equipped with a CCD camera using an excitation laser wavelength of 633 nm at an exposure time of 60 s. For recording spectra, a 21/Q/1 quartz cuvette (wavelength range 170-2700 nm; optical path length 1 mm), purchased from Starna Pty Ltd., was used. Freshly prepared electrolyte solution samples were loaded into the cuvette and tightly sealed with a polytetrafluoroethylene stopper before withdrawal from the argon glove box for the analysis.

Scanning Electron Microscopy (SEM) analysis was undertaken using a JEOL JSM-7001F FEG-SEM at an accelerating voltage of 15 kV, emission current of 108 μA, probe current corresponding to an instrumental setting of "7" and objective lens aperture corresponding to an instrumental setting of "4". Energy dispersive X-ray spectroscopic (EDS) analysis was undertaken using an Oxford Instruments AZtec X-ray analysis system attached to the SEM

instrument. Sample for the SEM/EDS analysis was prepared by chronopotentiometric reduction (-7 mA cm^{-2}, on the 0.114 cm^2 surface area of Cu wire for 12 h) of the 0.2 M $Mg(BH_4)_2$ + 0.4 M LiTFSI solution in DME using a copper wire working electrode. After reduction, the cell was opened in the glove box. The sample (after washing with DME) was attached to the SEM supporting stub with a double-side conducting carbon tape and kept inside the glove-box (*ca.* 30 min) before being loaded into the microscope.

X-ray Diffraction (XRD) analysis was performed using a Bruker D8 Advance X-ray diffractometer equipped with a Cu K_α radiation source (operated at 40 mA and 40 kV) with wavelength of 1.5406 Å. Match! software was used for the data processing. XRD analysis was undertaken on the same sample that was first used for the SEM/EDS characterisation.

^{7}Li and ^{11}B nuclear magnetic resonance (NMR) data were recorded using a Bruker Avance III 400 MHz spectrometer at ambient temperature, as well as at 0, -20 and -50 °C. Electrolyte solutions were introduced to the NMR tubes and securely sealed insides the glove-box.

X-ray photoelectron spectroscopic (XPS) analysis was undertaken using a Thermo Scientific Nexsa Surface Analysis System equipped with a hemispherical analyser and an X-ray source providing a monochromatic Al K_α X-ray (1486.6 eV) incident radiation (72 W, 6 mA and 12 kV, 400 μm × 800 μm spot). The pressure in the analysis chamber was below 5.0×10^{-9} mbar. Survey and high-resolution spectra were recorded at analyser pass energies of 150 eV and 50 eV and step sizes of 1.0 eV and 0.1 eV, respectively. Surface charging was compensated using a low-energy dual-beam (ion and electron) flood gun. The Avantage software (Version 5.9921) was used for data processing and the binding energy scale was referenced to the aliphatic C 1s signal at 284.8 eV.

Conductivity of the selected electrolyte solutions was measured in a custom-built dip-cell, assembled with two Pt electrodes separated by *ca.* 5 mm. The measurements were undertaken at frequencies between 1 Hz and 10 MHz with an amplitude of 10 mV using an alternating current impedance spectroscopy utilising a BioLogic MTZ-35 instrument equipped with a MTZ frequency response analyser. The cell constant of 1304 cm^{-1} was measured using a standard 0.01 M KCl aqueous solution at 25 °C, which was assumed to have a conductivity of 1.41 mS cm^{-1}. Conductivity was calculated using the real impedance value at the zero imaginary impedance component in the Nyquist plots.

Results and discussion

Optimisation of the electrolyte composition

Inspired by the previous developments of Mohtadi *et al.*[18], mixed magnesium-lithium electrolyte systems in DME solvent with varied concentrations of the borohydride anion were investigated herein. The kinetics of the magnesium(0/2+) process on a Cu disk electrode was very slow when using only $Mg(BH_4)_2$ as an electrolyte, corresponding to the oxidative stripping current density of only 0.05 mA cm^{-2} for a negative switching potential of -0.8 V *vs.* $Mg^{0/2+}$; the coulombic efficiency (CE) in this case was *ca.* 62% (Figure 1 inset). Introduction of lithium salts into the $Mg(BH_4)_2$ electrolyte solutions accelerated the kinetics of the magnesium reduction/oxidation by more than an order of magnitude. Replacing $LiBH_4$ with LiTFSI was even more advantageous in terms of both electrochemical kinetics and coulombic efficiency of the $Mg^{0/2+}$ cycling (Figure 1). Specifically, the $j_{-0.8}$ values in 10th voltammetric cycles were 4 mA cm^{-2} and 28 mA cm^{-2}, and the CE values calculated for the 10th voltammetric cycles were 85 and 89% for the 0.18 M $Mg(BH_4)_2$ + 0.4 M $LiBH_4$ and 0.18 M $Mg(BH_4)_2$ + 0.4 M LiTFSI systems, respectively.

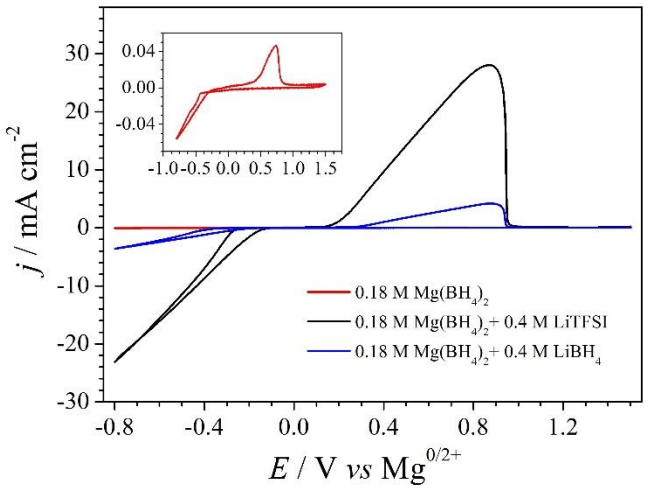

Figure 1. Cyclic voltammograms (10th cycles, scan rate 0.020 V s^{-1}) of a Cu disk electrode in Ar-saturated DME solutions containing 0.18 M $Mg(BH_4)_2$ (*red*), 0.18 M $Mg(BH_4)_2$ + 0.4 M $LiBH_4$ (*blue*) and 0.18 M $Mg(BH_4)_2$ + 0.4 M LiTFSI (*black*). Inset shows enhanced plot for the data obtained with 0.18 M $Mg(BH_4)_2$. Currents are normalised to the geometric surface of the electrode.

Although the 0.18 M $Mg(BH_4)_2$ + 0.4 M LiTFSI in DME system performs reasonably well for the Mg^0 deposition/stripping (Table 1), it would be desirable to minimise the concentration of borohydride. To this end, the effect of the $Mg(BH_4)_2$ concentration in the electrolyte solution on the electrochemical performance was examined. Keeping the LiTFSI concentration constant at 0.4 M, the concentration of $Mg(BH_4)_2$ was varied within a 0.01-0.36 M range and the electrochemical behaviour was investigated by cyclic voltammetry. Similar experiments were also undertaken with constant $Mg(BH_4)_2$ concentration of 0.2 M, while varying the amount of LiTFSI present. Data derived from 10^{th} voltammetric cycles of these tests are summarised in Figure 2, while those for the first cycles are shown in Figure S1 (all data are summarised in Table S1 and S2). We also note that magnesium cycling in the mixed $Mg(BH_4)_2$ + LiTFSI electrolyte solutions in DME is highly stable and the performance metrics do not change to a significant extent after 10^{th} cycles (Figure S2).

The metal stripping current density in cyclic voltammetry almost linearly increased with the $Mg(BH_4)_2$ concentration in solutions containing 0.4 M LiTFSI, until reaching a maximum at 0.2 M, and slightly decreased when more magnesium borohydride was introduced; this trend was maintained throughout cycling (Figure 2c and Figure S1c). Similarly, close to linear dependence of the current density on the concentration of LiTFSI was found in the 0.1-0.4 M range with no further improvements achieved when higher amounts of the salt were added to the 0.2 M $Mg(BH_4)_2$ solutions (Figure 2d and Figure S1d). Higher amounts of magnesium borohydride favoured increased coulombic efficiency of the process, which approached *ca.* 90% in 10^{th} voltammetric scans at $Mg(BH_4)_2$ concentrations higher than 0.18 M (Figure 2e). At the same time, the CE did not change significantly within the [LiTFSI] range of 0.1-0.4 M, but slightly deteriorated at higher concentrations (Figure 2f). These results indicate that the best performance requires an optimal ratio between $Mg(BH_4)_2$ and LiTFSI, which approximate value was determined herein as $[Mg(BH_4)_2]$: [LiTFSI] = 1 : 2 (Figure 2b-c).

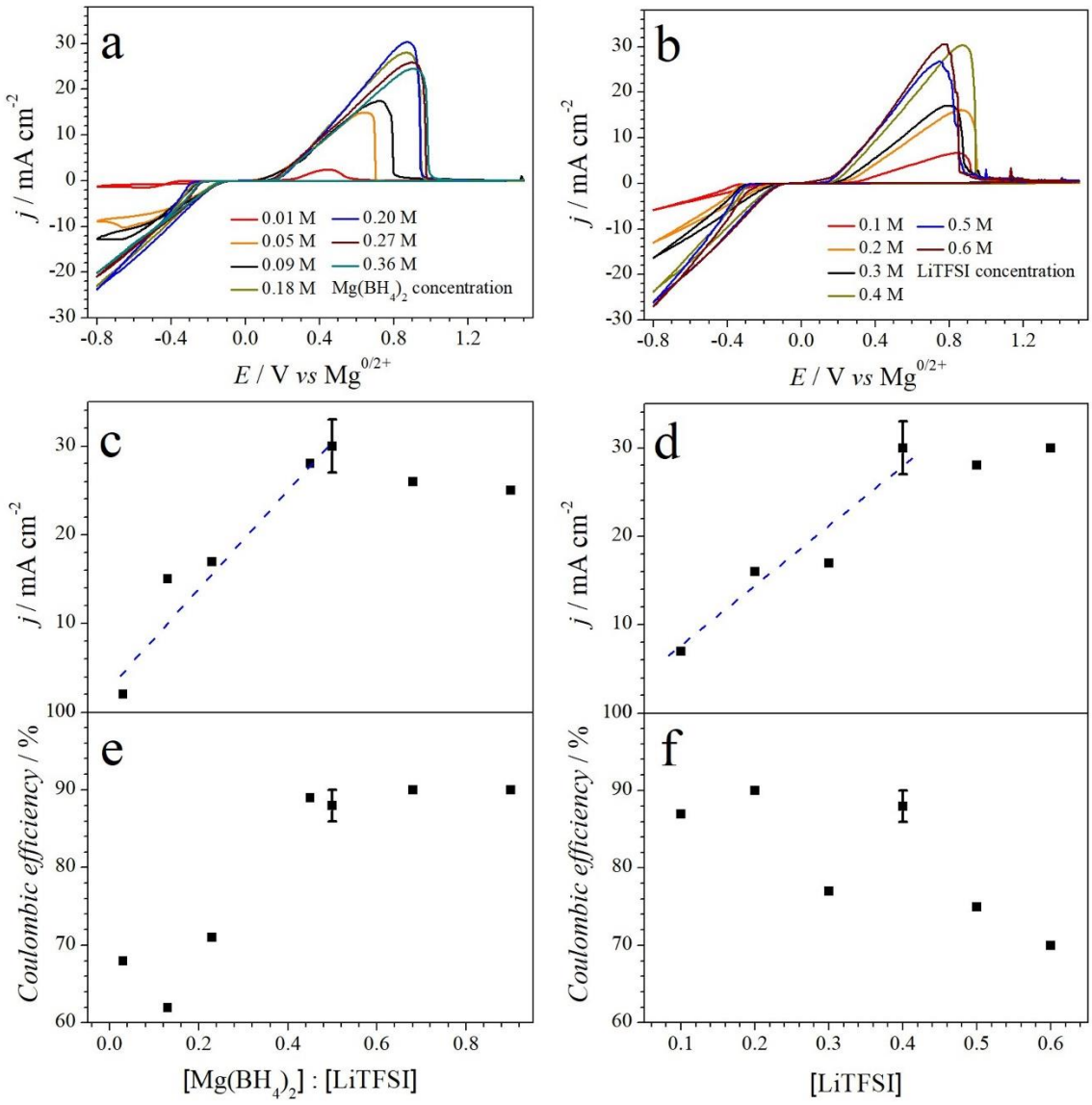

Figure 2. (a-b) Cyclic voltammograms (10^{th} cycles, scan rate v = 0.020 V s^{-1}; E_{nr} = -0.8 V *vs.* $Mg^{0/2+}$) of a Cu disk electrode in Ar-saturated DME solutions containing (a) 0.4 M LiTFSI with varied concentrations of $Mg(BH_4)_2$, and (b) 0.2 M $Mg(BH_4)_2$ with varied concentrations of LiTFSI (see figure). Corresponding (c-d) oxidation peak current densities for the magnesium stripping, and (e-f) coulombic efficiencies (calculated as a ratio of the oxidative to the reductive charges measured during voltammetric sweeps). Datapoints with error bars show mean ± standard deviation for n = 3 independent repeats of the experiment. Dashed lines in panels c and d are guides to the eye.

To obtain deeper insights into the effects of the electrolyte composition on the $Mg^{0/2+}$ electrochemistry, a range of solutions containing different concentrations of $Mg(BH_4)_2$, $LiBH_4$, $Mg(TFSI)_2$ and LiTFSI with varied $[BH_4^-]$: $[TFSI^-]$ ratio but with the $[Mg^{2+}]$: $[Li^+]$ ratio kept close to the apparently optimal value of 1 : 2 identified above was investigated; the total Mg^{2+} concentration was kept constant at 0.2 M (Figure 3, Figure S3 and Table S3). Although some

variability was observed at low borohydride concentrations, it was found that reasonably high coulombic efficiency values of 85% and higher are possible even at very low $[BH_4^-]$: $[TFSI^-]$ ratio of *ca* 0.03, *viz* $[BH_4^-]$ = 0.02 M. However, a significant enhancement in the current density was observed when the $[BH_4^-]$: $[TFSI^-]$ ratio was increased to 0.14 (corresponding to 0.1 M BH_4^- under the conditions considered) and beyond. Most consistent and highest performance results were obtained with the borohydride to bis(trifluoromethanesulfonyl)imide ratio of ≥0.3 provided by the $[BH_4^-]$ concentration of 0.18 M. It is important to note that this borohydride concentration value is vastly higher than the highest possible concentration of the H_2O impurity of ≤0.0003 M in the examined electrolyte solutions as determined by Karl-Fisher titration. Hence, it is concluded that the role of borohydride is not limited to water scavenging, but this anion also promotes the $Mg^{0/2+}$ cycling *via* a different mechanism. It is also noted that the excessively high concentration of borohydride anion of 0.6 M ($[BH_4^-]$: $[TFSI^-]$ = 3) decreases the current density of the magnesium plating/stripping, but maintains high coulombic efficiency of the process (Figure 3, Table S3). The limiting case of the $TFSI^-$-free solutions provided very low rates of the $Mg^{0/2+}$ process, as discussed above (Figure 1 and 3).

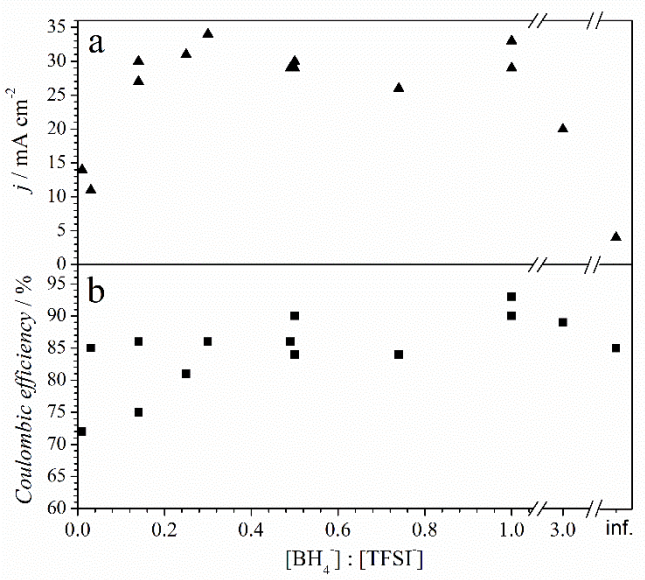

Figure 3. (a) Oxidation peak current densities for the magnesium stripping, and (b) coulombic efficiencies of the $Mg^{0/2+}$ cycling derived from 10th cycles of cyclic voltammograms (v = 0.020 V s^{-1}) recorded down to -0.80 V *vs.* $Mg^{0/2+}$ using a Cu electrode in Ar-saturated DME solutions containing different concentrations of $Mg(BH_4)_2$, $LiBH_4$, $Mg(TFSI)_2$ and LiTFSI with a *ca.* $[Mg^{2+}]$: $[Li^+]$ = 1 : 2 ratio and varied $[BH_4^-]$: $[TFSI^-]$ ratio (see Figures S3 and Table S3 for the extended experimental data). Coulombic efficiency was calculated as a ratio of the oxidative to the reductive charges measured during voltammetric sweeps.

In a separate set of experiments, the Cu electrode was replaced with platinum, which is routinely employed for Mg electrochemical cycling studies (Table 1). The change of the working electrode did not affect the coulombic efficiency to a significant extent, but substantially increased the current density (Table 1 and Figure S4). A plausible explanation of the observed change in the electrochemical kinetics is more homogeneous nucleation of magnesium(0) on a noble metal surface as compared to copper. However, detailed understanding of the electrode effects requires deeper electrochemical and physical characterisation studies, which go beyond the purposes of the present work. Herein, we only aim to highlight that even further improvements are possible through optimisation of the working electrode substrate. In fact, the metrics of the electrochemical $Mg^{0/2+}$ cycling, *viz.* the reduction/stripping rates and coulombic efficiency, provided by the 0.2 M $Mg(BH_4)_2$ + 0.4 M LiTFSI electrolyte solution in DME with platinum electrode are among the highest reported to date (Table 1). Additionally, cyclic voltammograms at different negative switching potentials with Pt electrode with the 0.2 M $Mg(BH_4)_2$ + 0.4 M LiTFSI (DME) system were compared (Figure S4). No significant effect of the switching potential on the coulombic efficiency of the process was observed (Table S4).

Characterisation of electrodeposited material

To prove the occurrence of magnesium deposition on the electrode during the electrochemical cycling, a chronoamperometric experiment was performed using optimised 0.2 M $Mg(BH_4)_2$ + 0.4 M LiTFSI electrolyte solution. Analysis of the deposit produced on the Cu electrode during 12 h galvanostatic deposition by energy dispersive X-ray spectroscopy and X-ray diffraction confirmed that Mg-metal is by far the dominating component of the electrochemically generated material (Figure S5). This was corroborated by voltammetric data recorded for 0.4 M LiTFSI in the absence of magnesium salts, which produced essentially featureless curves (Figure S6) confirming negligible contribution of the $Li^{0/+}$ process to the electrodeposition processes occurring with the $Mg(BH_4)_2$ + LiTFSI hybrid system.

To further investigate the composition of the Mg deposits, the material produced on the surface of a Cu electrode after recording 10 voltammetric cycles (as in Figure 2a-b) and stopping at -0.8 V *vs.* $Mg^{0/2+}$ in 0.2 M $Mg(BH_4)_2$ + 0.4 M LiTFSI (DME) was probed by X-ray photoelectron spectroscopy (XPS) (Figure S7). Spectra recorded before argon ion beam etching exhibited detectable copper signals indicating that the produced magnesium layer, clearly detected by XPS, is either very thin or non-continuous (Figure S7k). Examination of the Mg 1s and especially Mg KLL spectra suggests that magnesium is majorly present in the 2+ oxidation

state at the surface, but also after etching (Figure S7h-i). This is inconsistent with the XRD data and especially high coulombic cycling efficiency (if Mg^{2+} species were formed during electrodeposition, they could not be effectively stripped during oxidative sweeps). The appearance of these Mg^{2+} species is therefore attributed to the experimental limitations in handling the electrode prior to XPS characterisation (minor contamination of O_2 and/or argon-ion-beam-induced effects).[24] More importantly, no Li 1s signals were detected, neither at the surface nor after etching (Figure S7e) confirming that significant amounts of lithium-based species are not incorporated in the deposit (only Mg 2p and Mg plasmon loss peaks were observed in the relevant binding energy range[25, 26]). No detectable nitrogen and sulphur signals were found either (Figure S7b-c). At the same time, B 1s and F 1s signals that can be attributed to the [B-O] (192 eV)[27] and MgF_2 (686 eV)[28] species were clearly detectable at the surface, both of which rapidly disappeared after very short etching (Figure S7f-g). Overall, XPS analysis indicates that the major component of the produced deposit is magnesium, while the surface is modified by a very thin interfacial layer based on MgF_2 and oxidised boron, but not lithium species.

Spectroscopic analysis of the electrolyte solutions

The coordination environment of the Mg^{2+} ions in the electrolyte solution is one factor that can influence the electrochemical performance.[7] There are three species that can coordinate to Mg^{2+} in the investigated system: the DME solvent, as well as BH_4^- and $TFSI^-$ anions. To probe the coordination of ions in the system of interest, Raman and ^{7}Li NMR spectroscopic characterisation of the DME solutions of $Mg(BH_4)_2$ + LiTFSI and $Mg(TFSI)_2$ + $LiBH_4$ combinations, containing equal concentrations of BH_4^- and $TFSI^-$ ions, as well as of the individual solutions of magnesium and lithium borohydrides, was performed.

Raman spectra of $Mg(BH_4)_2$ and $LiBH_4$ solutions in DME exhibited the same band at 2205 cm^{-1}, which is attributed in the literature to bridging B-H vibrations of the metal ion-borohydride complex, but differed notably in the position of the signal at higher Raman shift values, that can be ascribed to terminal B-H vibrations.[9, 29] However, spectra of the solutions of $Mg(BH_4)_2$, $Mg(BH_4)_2$ + LiTFSI and $Mg(TFSI)_2$ + $LiBH_4$ are all identical within experimental error (Figure 4a). This observation suggests a ligand exchange between $Mg(TFSI)_2$ and $LiBH_4$, and the presence of Mg^{2+}-BH_4^- complexes in all Mg^{2+} solutions. This was further confirmed by the ^{7}Li NMR spectra of the relevant Li^+ containing systems. Indeed, the Li^+ ion environment is different in the individual DME solutions of LiTFSI and $LiBH_4$, but identical in the LiTFSI, $Mg(BH_4)_2$ + LiTFSI and $Mg(TFSI)_2$ + $LiBH_4$ solutions (Figure 4b). At

the same time, Raman analysis suggests that $TFSI^-$ anions do not coordinate neither to Li^+ nor to Mg^{2+} in DME, since spectra collected for all solutions of interest herein with this anion present exhibited an identical, sole band at *ca.* 742 cm^{-1} (Figure S8). The latter was attributed to uncoordinated $TFSI^-$, while bis(trifluoromethanesulfonyl)imide coordinated to a metal ion should produce a signal at 753 cm^{-1},[29, 30] which was not detected for any solution herein.

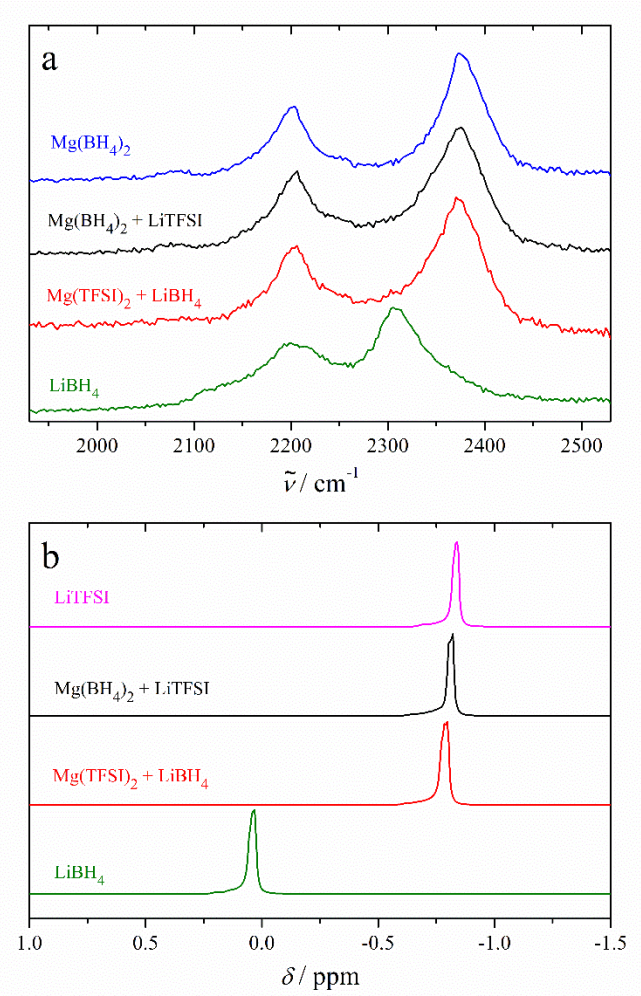

Figure 4. Spectroscopic characterisation of the electrolyte solutions: (a) Raman spectra of DME containing 0.2 M $Mg(BH_4)_2$ (*blue*), 0.2 M $Mg(BH_4)_2$ + 0.4 M LiTFSI (*black*), 0.2 M $Mg(TFSI)_2$ + 0.4 M $LiBH_4$ (*red*), and 0.4 M $LiBH_4$ (*green*) in the region corresponding to the BH_4^- anions (data are corrected for the spectrum of pure DME), and (b) ^{7}Li NMR spectra of DME containing 0.4 M LiTFSI (*magenta*), 0.2 M $Mg(BH_4)_2$ + 0.4 M LiTFSI (*black*), 0.2 M $Mg(TFSI)_2$ + 0.4 M $LiBH_4$ (*red*), and 0.4 M $LiBH_4$ (*green*).

Additional ^{7}Li and ^{11}B NMR experiments were performed at low temperatures (0, -20 and -50 °C) for $LiBH_4$ and $Mg(TFSI)_2$ + $LiBH_4$ solutions in attempt to probe reversible complex formation, which might be undetectably rapid at ambient temperature. ^{7}Li NMR spectra did not show any remarkable effects of temperature for both solutions examined,

similarly to the ^{11}B NMR data obtained for the $LiBH_4$ solution (Figure S9a-c). However, the ^{11}B NMR spectra of the $Mg(TFSI)_2$ + $LiBH_4$ solution demonstrated pronounced broadening at lower temperatures (Figure S9d). This effect might be associated with deceleration of the reorientation of coordinated BH_4^- with the highest activation energy, and indicate the presence of various borohydride complexes and/or gradual freezing of the complex equilibria. Precipitation of the electrolyte salts, which might also induce the observed effects, is unlikely to be a significant factor in these experiments as the ^7Li NMR spectra did not show any pronounced temperature dependence. Overall, the low temperature NMR measurements corroborate the ambient temperature data, *viz.* coordination of BH_4^- to Mg^{2+}.

The outcomes of the spectroscopic analysis undertaken herein are in line with those of the recent NMR spectroscopic study by Shao *et al.*[7] who suggested that $Mg(BH_4)_2$ in DME forms a dimeric species, $Mg_2(BH_4)_4(DME)_3$, where each Mg^{2+} is coordinated to two BH_4^- anions, a bidentate DME ligand and a monodentate DME ligand bridging to the other Mg^{2+} ion. Recent theoretical analysis of the most stable structures of $Mg(BH_4)_2$ and $Mg(TFSI)_2$ in DME and diglyme (1-methoxy-2-(2-methoxyethoxy)ethane; DGM) solvents confirmed that BH_4^- is a strongly bonding and $TFSI^-$ is a weakly bonding ligand to Mg^{2+}. The strong interaction between Mg^{2+} and BH_4^- precludes solvent mediated dissociation of Mg^{2+} and BH_4^- in ethereal solvents.[31, 32] Our results are also consistent with other reports indicating that ethereal solvents displace $TFSI^-$ ions from the Mg^{2+} or Li^+ coordination sphere.[14, 29] However, spectroscopic observations discussed above (Figure 4) are in contrast to those of Xu *et al.*[9] and Watkin *et al.*[14] who suggested the emergence of the Raman signal of uncoordinated BH_4^- anion in the $Mg(BH_4)_2$ solutions in diglyme upon introduction of high concentrations of tris(2H-hexafluoroisopropyl)borate additive and in PEGylated-ionic liquids, respectively, due to displacement of BH_4^- from the coordination sphere of Mg^{2+}. Hence, the presence of uncoordinated borohydride cannot be invoked to explain the improved electrochemical magnesium(0/2+) cycling in the mixed Mg^{2+}-Li^+-$TFSI^-$-BH_4^- electrolyte solutions in DME.

New insights into the roles of auxiliary ions

To further probe the different roles of the supplementary ions in the $Mg(BH_4)_2$-based mixed electrolytes, we tested the $Mg^{0/2+}$ cycling in solutions where Li^+ or $TFSI^-$ were replaced with $P_{6,6,6,14}^+$ or $BHfip^-$, respectively (see experimental for full description of these ions). Additionally, pure magnesium-based electrolyte solutions containing $Mg(BH_4)_2$ and $Mg(TFSI)_2$ were examined. Replacement of $TFSI^-$ with the "bulkier" borate ester anion, $BHfip^-$, hardly effected cycling, neither using copper electrode nor the higher-performing platinum

(Figure 5a and Table S5). This result indicates that the $TFSI^-$ anions do not present the indispensable component required for the effective magnesium electroreduction/oxidation, and can be replaced with another auxiliary anionic species.

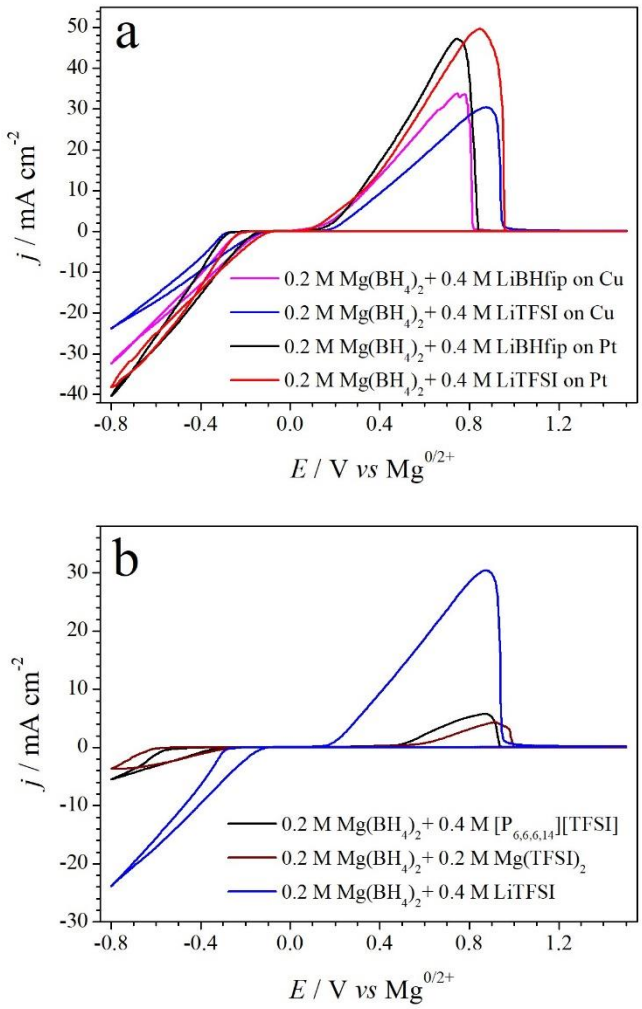

Figure 5. Effects of the chemical nature of (a) anion and (b) cation on the $Mg^{0/2+}$ voltammetric cycling (10^{th} cycles, scan rate 0.020 V s^{-1}) with a (a) Pt and (a, b) Cu disk electrodes in Ar-saturated DME solutions. Electrolyte compositions were: (a) 0.2 M $Mg(BH_4)_2$ + 0.4 M LiBHFip (*purple* and *black*) and 0.2 M $Mg(BH_4)_2$ + 0.4 M LiTFSI (*blue* and *red*); and (b), 0.2 M $Mg(BH_4)_2$ + 0.2 M $Mg(TFSI)_2$ (*red*) , 0.2 M $Mg(BH_4)_2$ + 0.4 M $P_{6,6,6,14}TFSI$ (*black*), and 0.2 M $Mg(BH_4)_2$ + 0.4 M LiTFSI (*blue*). In panel (a), data were collected using Pt (*black* and *red*) and Cu (*blue* and *purple*) electrodes.

Much more significant effects were observed when Li^+ cations were not present in the electrolyte solution (Figure 5b, Table S6). The monometallic Mg^{2+}-based solutions exhibited very poor deposition kinetics and coulombic efficiency compared to the $Mg(BH_4)_2$ + LiTFSI system. Experiments with the chemically very different, and bulky, phosphonium cation

$P_{6,6,6,14}^+$ also produced much worse performance as compared to the results obtained in the presence of Li^+ and otherwise identical system components (Figure 5b).

Overall, the results obtained herein collectively highlight a non-borohydride lithium salt as a key component of the mixed electrolyte systems that enables fast and reversible $Mg^{0/2+}$ cycling in the compositions like $Mg(BH_4)_2$ + LiTFSI, $Mg(TFSI)_2$ + $LiBH_4$ or $Mg(BH_4)_2$ + LiBHfip. It is important to emphasise again at this point that Li^+ on its own does not produce any significant charge-transfer processes in the potential region of interest (Figure S6). Hence, one might hypothesise that lithium ions might be responsible for generating electrochemically active magnesium species, for example, through the coordination of Li^+ ion to the neutral $Mg_2(BH_4)_4(DME)_3$ dimer to generate positively charged multinuclear complex, which reduction at the negatively charged surface might be more kinetically favourable.

At the same time, lithium salts might also interact with the negatively charged freshly electrodeposited magnesium and thereby facilitate subsequent Mg^0 deposition. To probe this, we investigated the redox behaviour of a magnesium ribbon electrode in the presence of different lithium salts by cyclic voltammetry (Figure 6). Control experiments were undertaken with a copper electrode (Figure S10).

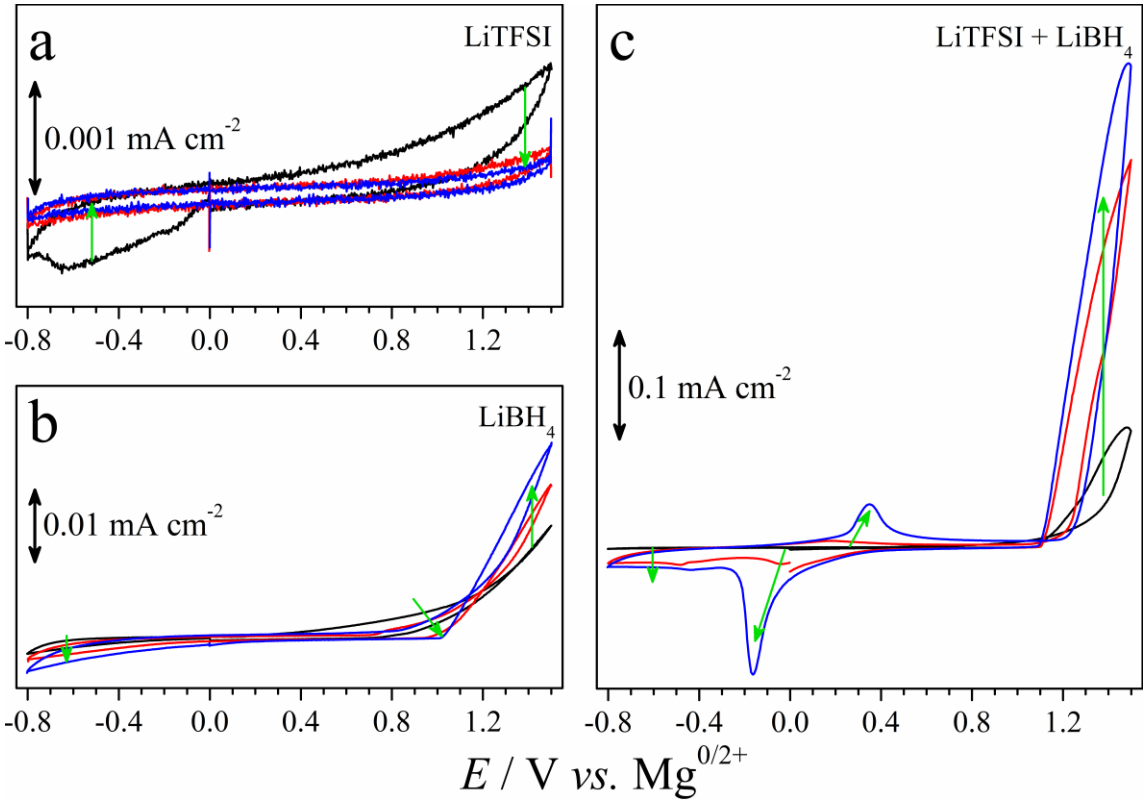

Figure 6. Cyclic voltammograms (v = 0.020 V s^{-1}; 1st cycle – *black*, 5th cycle – *red*, 10th cycle – *blue*; green arrows show the evolution of voltammograms with cycling) recorded using a Mg ribbon electrode in Ar-saturated DME solutions containing (a) 0.4 M LiTFSI, (b) 0.4 M $LiBH_4$, and (c) 0.2 M $LiBH_4$ + 0.2 M LiTFSI.

When using individual $LiBH_4$ and LiTFSI electrolytes, essentially featureless voltammograms were obtained with no $Mg^{0/2+}$ process detected (Figure 6a-b). Most likely this is associated with the naturally present thin (hydr)oxide layer on the magnesium electrode surface, which could not be completely removed even by abrasive polishing. At the same time, one might note a low intensity irreversible oxidation process commencing at potentials more positive than *ca* 1 V *vs.* $Mg^{0/2+}$ in the presence of $LiBH_4$ on a magnesium (Figure 6b), but not copper electrode (Figure S10b). We ascribe this process to kinetically hindered oxidative dissolution of magnesium, which could be then redeposited on the electrode surface, as confirmed by slow increase in the reductive currents at potentials more negative than 0 V *vs.* $Mg^{0/2+}$ with cycling (Figure 6b). Similar interpretation of the detected oxidative process was proposed by Senoh *et al.*[33] Most interestingly, combination of LiTFSI and $LiBH_4$ salts substantially enhanced redox activity of the magnesium electrode and enabled detection of a well-defined redox process around 0 V *vs.* $Mg^{0/2+}$ (Figure 6c). We interpret these observations by partial removal of the MgO_xH_y by the lithium borohydride–bis(trifluoromethanesulfonyl)imide combination of salts producing a favourable surface for the Mg^0 plating. One of the important roles of borohydride is likely chemical reduction of the oxygen-containing species, which is circumstantially confirmed by the presence of oxidised boron on the electrode surface (Figure S7f), while dissolution of the products of the reduction is facilitated by the Li^+ + $TFSI^-$ combination of ions. Since all of the supplementary ionic species participate in the process, their ratio will likely strongly affect the performance, as demonstrated above (Figure 2). Furthermore, given the lack of any evidence of the significant interactions of Li^+ and $TFSI^-$ with Mg^{2+} and BH_4^- in the solution (Figure 4 and discussions above) as well as of the incorporation of lithium-, fluorine- and boron-based species into the Mg^0 electrodeposit (Figures S7), we conclude that activation of the redox active magnesium surface (Figure 6) is the major origin of the promoting effect of supplementary Li^+, $TFSI^-$, and BH_4^- ions on the electrochemical $Mg^{0/2+}$ cycling.

Conclusion

In summary, efficient $Mg^{0/2+}$ cycling at high coulombic efficiencies has been achieved through combination and investigation of the $Mg(BH_4)_2$- and LiTFSI-based electrolyte system using DME solvent and either copper or platinum as an electrode. The use of the 0.2 M $Mg(BH_4)_2$ + 0.4 M LiTFSI electrolyte combination enabled outstanding rates of the magnesium electrodeposition and stripping, while platinum electrode provided even better results than those obtained with copper. Results indicate that borohydride anion is essential for magnesium cycling, but $Mg(BH_4)_2$ alone is a poor performer; the best performance requires an optimal ratio between $Mg(BH_4)_2$ and LiTFSI, which approximate value was determined herein as $[Mg(BH_4)_2]$: [LiTFSI] = 1 : 2. Raman and NMR studies of the $Mg(BH_4)_2$ + LiTFSI electrolyte system indicated that that BH_4^- ions coordinate to Mg^{2+}, and $TFSI^-$ is non-coordinating in the examined systems. Investigation into the roles of different ions on the $Mg^{0/2+}$ electrochemical cycling highlights the cumulative role of Li^+ + BH_4^- + $TFSI^-$ ionic species, which facilitate formation of electrochemically active, non-passivated magnesium metal surface.

Supporting Information

SEM, XRD and XPS analysis of the Mg-deposited copper electrode, cyclic voltammograms recorded using a Cu and Pt disk electrode containing different concentrations of $Mg(BH_4)_2$, $LiBH_4$, $Mg(TFSI)_2$ and LiTFSI, Raman and NMR spectra of the electrolyte solutions

Acknowledgements

Authors are grateful to Dr Jacinta Bakker (Monash University) for the synthesis of $[P_{6,6,6,14}][TFSI]$ salt and to Dr Alasdair McKay (Monash University) for the low temperature NMR measurements. The authors acknowledge Australian Renewable Energy Agency (project DRM015) and Australian Research Council (Centre of Excellence CE140100012; Future Fellowship to ANS FT200100317) for the financial support, as well as Monash Centre for Electron Microscopy and Monash X-ray platform for the access to SEM, XRD and XPS facilities.

References

1. Muldoon, J.; Bucur, C. B.; Gregory, T., Fervent Hype behind Magnesium Batteries: An Open Call to Synthetic Chemists—Electrolytes and Cathodes Needed. *Angewandte Chemie International Edition* **2017,** *56* (40), 12064-12084.

2. Tuerxun, F.; Abulizi, Y.; NuLi, Y.; Su, S.; Yang, J.; Wang, J., High concentration magnesium borohydride/tetraglyme electrolyte for rechargeable magnesium batteries. *Journal of Power Sources* **2015,** *276*, 255-261.

3. Aurbach, D.; Lu, Z.; Schechter, A.; Gofer, Y.; Gizbar, H.; Turgeman, R.; Cohen, Y.; Moshkovich, M.; Levi, E., Prototype systems for rechargeable magnesium batteries. *Nature* **2000,** *407* (6805), 724-727.

4. Muldoon, J.; Bucur, C. B.; Oliver, A. G.; Sugimoto, T.; Matsui, M.; Kim, H. S.; Allred, G. D.; Zajicek, J.; Kotani, Y., Electrolyte roadblocks to a magnesium rechargeable battery. *Energy & Environmental Science* **2012,** *5* (3), 5941-5950.

5. See, K. A.; Liu, Y.-M.; Ha, Y.; Barile, C. J.; Gewirth, A. A., Effect of Concentration on the Electrochemistry and Speciation of the Magnesium Aluminum Chloride Complex Electrolyte Solution. *ACS Applied Materials & Interfaces* **2017,** *9* (41), 35729-35739.

6. Xiong, F.; Fan, Y.; Tan, S.; Zhou, L.; Xu, Y.; Pei, C.; An, Q.; Mai, L., Magnesium storage performance and mechanism of CuS cathode. *Nano Energy* **2018,** *47*, 210-216.

7. Shao, Y.; Liu, T.; Li, G.; Gu, M.; Nie, Z.; Engelhard, M.; Xiao, J.; Lv, D.; Wang, C.; Zhang, J.-G.; Liu, J., Coordination Chemistry in magnesium battery electrolytes: how ligands affect their performance. *Scientific Reports* **2013,** *3* (1), 3130.

8. Su, S.; NuLi, Y.; Wang, N.; Yusipu, D.; Yang, J.; Wang, J., Magnesium Borohydride-Based Electrolytes Containing 1-butyl-1-methylpiperidinium bis(trifluoromethyl sulfonyl)imide Ionic Liquid for Rechargeable Magnesium Batteries. *J. Electrochem. Soc* **2016,** *163* (13), D682-D688.

9. Xu, H.; Zhang, Z.; Li, J.; Qiao, L.; Lu, C.; Tang, K.; Dong, S.; Ma, J.; Liu, Y.; Zhou, X.; Cui, G., Multifunctional Additives Improve the Electrolyte Properties of Magnesium Borohydride Toward Magnesium–Sulfur Batteries. *ACS Appl. Mater. Interfaces* **2018,** *10* (28), 23757-23765.

10. Mohtadi, R.; Tutusaus, O.; Arthur, T. S.; Zhao-Karger, Z.; Fichtner, M., The metamorphosis of rechargeable magnesium batteries. *Joule* **2021,** *5* (3), 581-617.

11. Gregory, T. D.; Hoffman, R. J.; Winterton, R. C., Nonaqueous Electrochemistry of Magnesium: Applications to Energy Storage. *Journal of the Electrochemical Society* **1990,** *137* (3), 775-780.

12. Pilarska, A. A.; Klapiszewski, Ł.; Jesionowski, T., Recent development in the synthesis, modification and application of Mg(OH)2 and MgO: A review. *Powder Technology* **2017,** *319*, 373-407.

13. Tuerxun, F.; Yamamoto, K.; Hattori, M.; Mandai, T.; Nakanishi, K.; Choudhary, A.; Tateyama, Y.; Sodeyama, K.; Nakao, A.; Uchiyama, T.; Matsui, M.; Tsuruta, K.; Tamenori, Y.; Kanamura, K.; Uchimoto, Y., Determining Factor on the Polarization Behavior of Magnesium Deposition for Magnesium Battery Anode. *ACS Appl Mater Interfaces* **2020,** *12* (23), 25775-25785.

14. Watkins, T.; Kumar, A.; Buttry, D. A., Designer Ionic Liquids for Reversible Electrochemical Deposition/Dissolution of Magnesium. *Journal of the American Chemical Society* **2016,** *138* (2), 641-650.

15. Ma, Z.; Kar, M.; Xiao, C.; Forsyth, M.; MacFarlane, D. R., Electrochemical cycling of Mg in Mg[TFSI]2/tetraglyme electrolytes. *Electrochemistry communications* **2017,** *78*, 29-32.

16. Hebié, S.; Ngo, H. P. K.; Leprêtre, J.-C.; Iojoiu, C.; Cointeaux, L.; Berthelot, R.; Alloin, F., Electrolyte Based on Easily Synthesized, Low Cost Triphenolate–Borohydride Salt for High Performance Mg(TFSI)2-Glyme Rechargeable Magnesium Batteries. *ACS Appl. Mater. Interfaces* **2017,** *9* (34), 28377-28385.

17. Kang, S.-J.; Kim, H.; Hwang, S.; Jo, M.; Jang, M.; Park, C.; Hong, S.-T.; Lee, H., Electrolyte Additive Enabling Conditioning-Free Electrolytes for Magnesium Batteries. *ACS Applied Materials & Interfaces* **2019,** *11* (1), 517-524.

18. Mohtadi, R.; Matsui, M.; Arthur, T. S.; Hwang, S.-J., Magnesium Borohydride: From Hydrogen Storage to Magnesium Battery. *Angewandte Chemie International Edition* **2012,** *51* (39), 9780-9783.

19. Chang, J.; Haasch, R. T.; Kim, J.; Spila, T.; Braun, P. V.; Gewirth, A. A.; Nuzzo, R. G., Synergetic Role of Li+ during Mg Electrodeposition/Dissolution in Borohydride Diglyme Electrolyte Solution: Voltammetric Stripping Behaviors on a Pt Microelectrode Indicative of Mg–Li Alloying and Facilitated Dissolution. *ACS Applied Materials & Interfaces* **2015,** *7* (4), 2494-2502.

20. Tutusaus, O.; Mohtadi, R., Paving the Way towards Highly Stable and Practical Electrolytes for Rechargeable Magnesium Batteries. *ChemElectroChem* **2015,** *2* (1), 51-57.

21. Roy, B.; Cherepanov, P.; Nguyen, C.; Forsyth, C.; Pal, U.; Mendes, T. C.; Howlett, P.; Forsyth, M.; MacFarlane, D.; Kar, M., Lithium Borate Ester Salts for Electrolyte Application in Next-Generation High Voltage Lithium Batteries. *Advanced Energy Materials* **2021,** *11* (36), 2101422.

22. Kang, C. S. M.; Zhang, X.; MacFarlane, D. R., Synthesis and Physicochemical Properties of Fluorinated Ionic Liquids with High Nitrogen Gas Solubility. *The Journal of Physical Chemistry C* **2018,** *122* (43), 24550-24558.

23. Johnston, S.; Kemp, L.; Turay, B.; Simonov, A. N.; Suryanto, B. H. R.; MacFarlane, D. R., Copper-Catalyzed Electrosynthesis of Nitrite and Nitrate from Ammonia: Tuning the Selectivity via an Interplay Between Homogeneous and Heterogeneous Catalysis. *ChemSusChem* **2021,** *14* (21), 4793-4801.

24. Greczynski, G.; Hultman, L., Towards reliable X-ray photoelectron spectroscopy: Sputter-damage effects in transition metal borides, carbides, nitrides, and oxides. *Applied Surface Science* **2021,** *542*, 148599.

25. Kurth, M.; Graat, P. C. J.; Mittemeijer, E. J., Determination of the intrinsic bulk and surface plasmon intensity of XPS spectra of magnesium. *Applied Surface Science* **2003,** *220* (1), 60-78.

26. van Attekum, P. M. T. M.; Trooster, J. M., Bulk- and surface-plasmon-loss intensities in photoelectron, Auger, and electron-energy-loss spectra of Mg metal. *Physical Review B* **1979,** *20* (6), 2335-2340.

27. Il'inchik, E. A.; Volkov, V. V.; Mazalov, L. N., X-ray photoelectron spectroscopy of boron compounds. *Journal of Structural Chemistry* **2005,** *46* (3), 523-534.

28. Reuna, J.; Polojärvi, V.; Pääkkönen, P.; Lahtonen, K.; Raappana, M.; Aho, T.; Isoaho, R.; Aho, A.; Valden, M.; Guina, M., Influence of ex-situ annealing on the properties of MgF2 thin films deposited by electron beam evaporation. *Optical Materials* **2019,** *96*, 109326.

29. Watkins, T.; Buttry, D. A., Determination of Mg2+ Speciation in a TFSI−-Based Ionic Liquid With and Without Chelating Ethers Using Raman Spectroscopy. *The Journal of Physical Chemistry B* **2015,** *119* (23), 7003-7014.

30. Liu, T.; Danten, Y.; Grondin, J.; Vilar, R., Solvation of AgTFSI in 1-ethyl-3-methylimidazolium bis(trifluoromethylsulfonyl)imide ionic liquid investigated by vibrational spectroscopy and DFT calculations. *Journal of Raman Spectroscopy* **2016,** *47* (4), 449-456.

31. Hu, J. Z.; Rajput, N. N.; Wan, C.; Shao, Y.; Deng, X.; Jaegers, N. R.; Hu, M.; Chen, Y.; Shin, Y.; Monk, J.; Chen, Z.; Qin, Z.; Mueller, K. T.; Liu, J.; Persson, K. A., 25Mg NMR and computational modeling studies of the solvation structures and molecular dynamics in magnesium based liquid electrolytes. *Nano Energy* **2018,** *46*, 436-446.

32. Deetz, J. D.; Cao, F.; Wang, Q.; Sun, H., Exploring the Liquid Structure and Ion Formation in Magnesium Borohydride Electrolyte Using Density Functional Theory. *Journal of The Electrochemical Society* **2018,** *165* (2), A61-A70.

33. Senoh, H.; Sakaebe, H.; Sano, H.; Yao, M.; Kuratani, K.; Takeichi, N.; Kiyobayashi, T., Sulfone-Based Electrolyte Solutions for Rechargeable Magnesium Batteries Using 2,5-Dimethoxy-1,4-benzoquinone Positive Electrode. *Journal of The Electrochemical Society* **2014,** *161* (9), A1315-A1320.